sustainability

MDPI

Article

Thermal Characteristics and Temperature Distribution of Asphalt Mixtures Containing Residues from Municipal Solid Waste Incineration

Ling Xu [1,*], Mohsen Alae [1], Yinfei Du [2,*], Giuseppe Loprencipe [3], Paolo Peluso [3] and Laura Moretti [3]

[1] Key Laboratory of Road and Traffic Engineering of Ministry of Education, Tongji University, No. 4800 Cao'an Road, Jiading District, Shanghai 201804, China; mohsen_alae@tongji.edu.cn
[2] School of Civil Engineering, Central South University, Changsha 410075, China
[3] Department of Civil, Constructional and Environmental Engineering, Sapienza University of Rome, Via Eudossiana 18, 00184 Rome, Italy; giuseppe.loprencipe@uniroma1.it (G.L.); paolo.peluso@uniroma1.it (P.P.); laura.moretti@uniroma1.it (L.M.)
* Correspondence: lxu@tongji.edu.cn (L.X.); yfdu_csu@csu.edu.cn (Y.D.)

Abstract: As a sustainable substitute for non-renewable mineral resources and solid waste landfilling, municipal solid waste incineration residues (MSWIRs) are useful in road pavements. This study investigates the thermal characteristics and temperature distribution of flexible pavements containing MSWIRs with hollow microsphere structures. First, the volumetric properties of asphalt mixtures containing MSWIR fillers were measured. The effects of MSWIRs on the mixture's physical characteristics were investigated in terms of thermal conductivity, specific heat capacity, and thermal diffusivity. A three-dimensional finite element model incorporating surface thermal conditions was established and validated to analyze the internal temperature distribution and heat transfer behavior within the asphalt. Finally, the high-temperature conditions of summer were simulated in an indoor irradiation test to evaluate the risk of heat islands in urban areas. The results showed that the mixture containing MSWIRs exhibited a higher specific heat capacity (from 0.8385 to 0.9554 J/(kg·K)) and lower thermal conductivity (from 1.4356 to 1.1362 W/(m·K)) than the reference mixture with limestone filler. Therefore, it contributed to a lower heat flux distribution within the pavement. However, the increase in asphalt surface temperature caused by MSWIRs may exacerbate the urban heat island effect in the summer, which should be considered before using road materials containing MSWIRs.

Keywords: asphalt; MSWIR; thermal simulation; urban heat island; waste recycling

Citation: Xu, L.; Alae, M.; Du, Y.; Loprencipe, G.; Peluso, P.; Moretti, L. Thermal Characteristics and Temperature Distribution of Asphalt Mixtures Containing Residues from Municipal Solid Waste Incineration. *Sustainability* **2023**, *15*, 15612. https://doi.org/10.3390/su152115612

Academic Editor: Graziano Salvalai

Received: 19 September 2023
Revised: 27 October 2023
Accepted: 2 November 2023
Published: 4 November 2023

1. Introduction

Rapid economic development [1], human activity [2], and urbanization [3,4] generate billions of tons of solid waste in urban areas worldwide [5], and municipal solid waste incineration (MSWI) residues accompany this waste [6,7]. Given their size distribution and chemical composition [8], the geotechnical properties of MSWIRs can increase recycling potential in construction when used as light fillers and aggregates [9]. Therefore, the secondary use of MSWIRs as sustainable substitutes for solid waste landfilling [10,11] has been gaining increasing attention from civil engineers. Municipal solid waste undergoes a combustion and pulverization process at coal-fired power stations, where complex physical and chemical reactions occur [12] until the MSWI residues harden into fine-grained powder [13]. High-temperature gases (mainly carbon dioxide and nitrogen) in the combustion furnace can cause the MSWIRs to expand violently [14], generating a lightweight [15,16] and hollow microsphere structure [17,18].

The thermal characteristics of construction materials determine their temperature variation and distribution, influencing the environment of urban areas [19,20]. This thermal behavior affects the durability of building materials [21]. As a typical viscoelastic–plastic

material, asphalt is temperature-sensitive [22,23]. Higher air temperatures and solar radiation in the summer result in more absorption and heat transfer energy in pavement [24,25]. As a result, high temperatures worsen permanent deformation, rutting risk, and moisture damage [26,27]. From this perspective, investigations of thermal properties and behavior are important for predicting and designing pavement materials and structures [28]. As a composite material, asphalt contains different heat transfer channels because of its components (i.e., coarse aggregates, fillers, and asphalt) [29]. Researchers have evaluated the effect of graphite on the thermal properties of asphalt mixtures [30]. They have found that asphalt-specific heat capacity decreases while thermal conductivity and diffusivity increase with the addition of graphite [31]. In heating and cooling conditions, researchers have tested different mixture specimens with various void ratios [32–34]. Densely graded mixtures exhibit lower temperature-changing rates than porous mixtures. Chen et al. [35] proposed a multiscale finite element model to simulate a mixture's steady-state heat transfer process and investigated its thermal conductivity. Similarly, Mirzanamadi et al. [36] investigated the effects of void ratio and aggregate gradation and type on a mixture's thermal conductivity using a two-dimensional finite element model. Mu et al. calculated temperature fluctuations and heat flux within a type of road pavement from a numerical perspective [37]. Carbon fibers with high axial thermal conductivity were incorporated into mixtures by Jiang et al. to enhance heat conductivity channels [38]. In another study, the heat flow distribution and temperature field along carbon fibers were calculated using a finite element approach [39]. Researchers have also studied the heat transfer and thermal influencing factors of road pavement [40,41]. Conventional and alternative mixtures have been investigated using in situ measurements and numerical simulations [42,43]. However, the current research gaps, major difficulties, and challenges regarding MSWIRs can be summarized as follows:

(1) Research on the effects of MSWI residues with hollow microsphere structures on the thermal behavior of asphalt roads is still relatively limited;
(2) The numerical studies in the literature do not focus on the effects of MSWIRs with hollow microsphere structures on the thermal behavior of flexible pavements;
(3) The interaction between MSWIRs in asphalt and the environment has not been validated through field investigations.

Therefore, the objectives of the present work include the following:

(1) Investigating the use of MSWIRs as fillers in asphalt mixtures whose thermal characteristics must be measured;
(2) Developing a three-dimensional finite element model (FEM) to investigate temperature distributions;
(3) Analyzing the thermal resistance of asphalt mixtures with MSWIRs and their effectiveness in countering urban heat islands.

This study investigates the thermal properties and behavior of building materials, which are important for designing road pavement that can reduce the risk of rutting and moisture damage and counter urban heat island effects. Additionally, secondary raw materials in asphalt can balance environmental and thermal goals, facilitating sustainable solutions.

2. Materials and Methods

2.1. Materials

This study used a bitumen (#70 binder) compliant with JTG E20-2011 [44]. Table 1 lists its physical properties.

Table 1. Physical properties of #70 binder.

Property	Unit	Result	Technical Requirement	Test Method
Penetration, 25 °C, 100 g/5 s	0.1 mm	71.2	60–80	T 0604 [44]
Softening point	°C	46.3	≥45	T 0606 [44]
Ductility, 10 °C	cm	38	≥20	T 0605 [44]
Ductility, 15 °C	cm	>150	≥100	T 0605 [44]
Specific gravity (15 °C)	g/cm^3	1.039	-	T 0603 [44]

The limestone aggregates used in this study were divided into four sizes: 10–15 mm, 5–10 mm, 3–5 mm, and 0–3 mm. The basic properties of these aggregates are listed in Table 2. They were measured according to JTG E42-2005 [45].

Table 2. Basic properties of aggregates and fillers.

Aggregate Property	Bulk Relative Density (g/cm^3)	Apparent Relative Density (g/cm^3)	Water Absorption (%)
10–15 mm	2.704	2.735	0.45
5–10 mm	2.686	2.720	0.44
3–5 mm	2.635	2.743	1.41
0–3 mm	2.621	2.663	1.56
Filler property	Acronym	Appearance	Density (g/cm^3)
Limestone filler	LF	White powder	2.77
MSWI residue	MSWIR	Gray spherical particles	0.72

The MSWIR used in this study was produced and recycled after heavy-metal filtration in local incineration plants. The natural limestone filler was derived from grinding limestone aggregate. The maximum size of both the LF and MSWIR was 0.075 mm, and their properties are listed in Table 2.

We investigated the asphalt mixture SMA-13 because it is commonly used in the wearing layer of urban areas. According to the equal volume concept, the MSWIR replaces the LF with different LF-to-MSWIR mass ratios. The corresponding aggregate gradation of SMA-13 and the specific mass ratios of the fillers in the asphalt mixtures are listed in Table 3 (i.e., a control mixture and Mixtures #1 to #4, with increasing MSWIR content).

Table 3. Aggregate gradation of SMA-13 and mass ratios of fillers in asphalt mixtures [46].

Sieve size (mm)		16.0	13.2	9.5	4.75	2.36	1.18	0.6	0.3	0.15	0.075
Passing ratio by weight (%)		100	90.2	63.4	26.5	17.7	15.4	13.1	11.2	10.5	9.8
Mixture type		Control Mixture		Mixture #1		Mixture #2		Mixture #3		Mixture #4	
Mixture number		1		2		3		4		5	
Filler ratio (% by volume)	LF	100		75		50		25		0	
	MSWIR	0		25		50		75		100	
Mass ratio (% by weight)	LF	9.6		7.2		4.8		2.4		0	
	MSWIR	0		0.6		1.2		1.9		2.5	

2.2. Methods

Marshall's design method was employed to determine the bulk density (ρ), air voids (VV), air voids in mineral aggregate (VMA), and voids filled with asphalt (VFA) of SMA-13 according to [44]. The Marshall stability test was employed to measure the mechanical parameters of the asphalt [44], including the Marshall stability (MS) and flow (FL) values.

Using the transient-plane heat source method (Hot Disk-TP3500, Xiangtan Instrument Co., LTD, Xiang Tan City, China), the mixture's thermal conductivity (λ) was measured

with a thermal conductivity tester (DRE-2C). Before testing, each Marshall specimen was cut into several slices with smooth surfaces. Then, a testing probe with a thermal sensor was placed between two mixture slices in close contact (Figure 1); ten repeated experiments provided the average thermal conductivity.

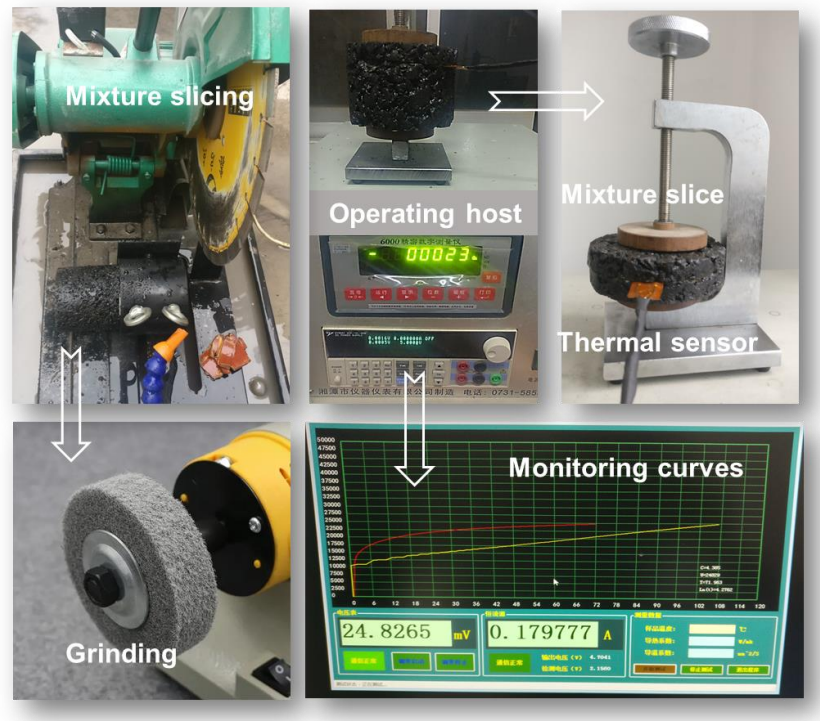

Figure 1. Thermal conductivity test set.

In this study, a specific heat capacity tester operated in accordance with a heat transfer method was used to measure the specific heat capacity of the asphalt (Figure 2). A Marshall specimen was placed in an incubator with a uniform temperature and then immersed in water in an insulated bucket. The specific heat capacity (c) value was calculated by judging when the Marshall specimen reached a temperature equilibrium state.

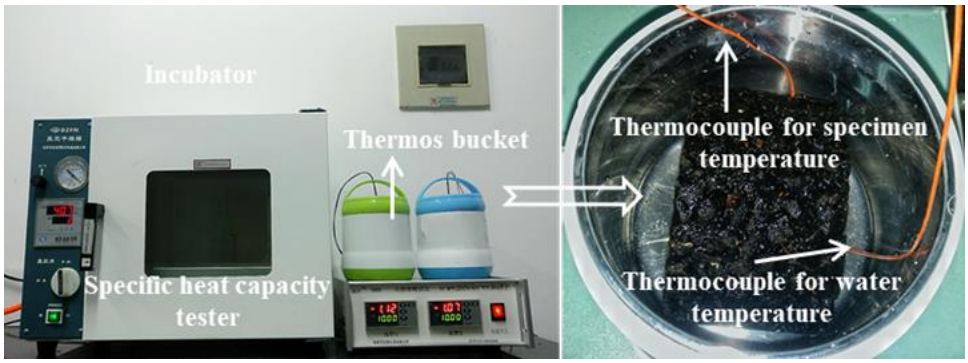

Figure 2. Set-up for heat capacity measurement.

Combining the mechanical and thermal properties of the mixtures, Equation (1) provides the thermal diffusivity (α, mm^2/s)

$$\alpha = \frac{\lambda}{\rho c} \quad (1)$$

where λ is the thermal conductivity (W/m K), ρ is the gross bulk density, g/cm^3, and c is the specific heat capacity of the mixture, J/(kg·K).

The ABAQUS software version 2023 product was used to develop a three-dimensional extended FEM of the asphalt mixture to simulate thermal conduction. The boundary condition parameters, contact form, and geometric assembly were like those in the experimental set: (1) The sample model was isotropic and homogeneous in terms of measured density (with a Young's modulus equal to 6000 MPa and a Poisson's ratio equal to 0.35), and the thermal properties of the material were determined based on the above thermodynamic tests. (2) The interfacial bonding was simulated with a tie constraint. (3) Fixed support and field thermal conditions were determined for the topmost layer of the road pavement. Each modeled specimen was a cylinder consisting of 8-node linear bricks with hourglass control (C3D8R) for the mesh conditions.

The thermal FEM of the asphalt pavement was based on the measured volumetric and thermal parameters of the asphalt mixture. The boundary condition of the model was set as thermally insulated, in addition to the road surface where convective heat exchange occurs. According to subroutines in the software, the surface thermal field of the pavement was set in terms of solar radiation heat flux density ($q_{\_solar}(t)$), total and maximum daily solar radiation (Q and q_0, respectively), and heat flux transfer (Figure 3).

1. The DFLUX subroutine calculated the daily solar radiation absorbed by the surface assuming an absorption coefficient equal to 0.88–0.95. Equations (2) and (3) describe the solar radiation tendency

$$q_{solar}(t) = \begin{cases} 0,\ 0 \le t \le 12 - b/2 \\ q_0 \cos(\pi(t-12)/b),\ 12 - b/2 \le t \le 12 + b/2 \\ 0,\ 12 + b/2 \le t \le 24 \end{cases} \quad (2)$$

$$q_0 = \frac{\pi}{24} 12Q/b \quad (3)$$

where b is the effective sunshine hour (hour), and t is the time.

2. Equation (4) describes the surface heat transfer according to the FILM subroutine, which results from the temperature difference between air and the asphalt surface

$$q_{air}(t) = h_c \left[T_{air}(t) - T_{surface}(t) \right] \quad (4)$$

$$T_{air}(t) = \overline{T_a} + T_m \left[0.96 sin \frac{\pi(t-9)}{12} + 0.14 sin \frac{\pi(t-9)}{6} \right] \quad (5)$$

$$h_c = 3.7w + 9.4 \quad (6)$$

where $q_{air}(t)$ is the transferred surface heat flux from external air at time t, W/m^2; h_c is the heat transfer coefficient, W/m^2 °C; $T_{air}(t)$ is the air temperature, °C; $\overline{T_a}$ is the daily average air temperature, °C; T_m is the daily excursion of the air temperature, °C; $T_{surface}(t)$ is the temperature of the asphalt surface, °C; and w is the daily average wind speed, m/s.

3. Based on the Stefan–Boltzmann law, Equation (7) was used to calculate the surface radiation of the pavement ($q_{rad}(t)$)

$$q_{rad}(t) = 5.67 \times 10^{-8} \varepsilon \left[\left(T_{surface}(t) + 273 \right)^4 - \left(T_{air}(t) + 273 \right)^4 \right] \quad (7)$$

where ε is the surface emissivity of the asphalt.

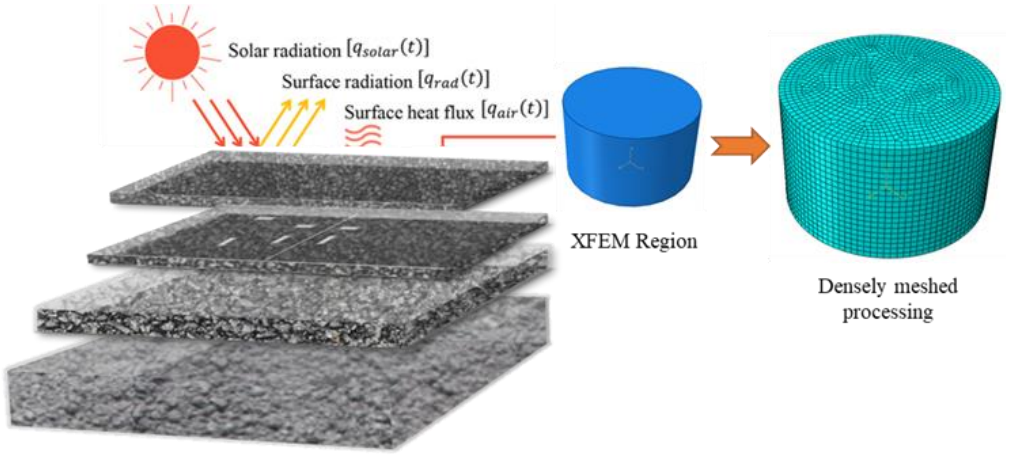

Figure 3. Thermal model of asphalt pavement and boundary conditions.

Indoor irradiation and temperature monitoring were conducted to simulate extremely high-temperature conditions (Figure 4). Sixteen incandescent 275 W lamps were placed 90 cm above the Marshall specimens to simulate solar radiation in summer.

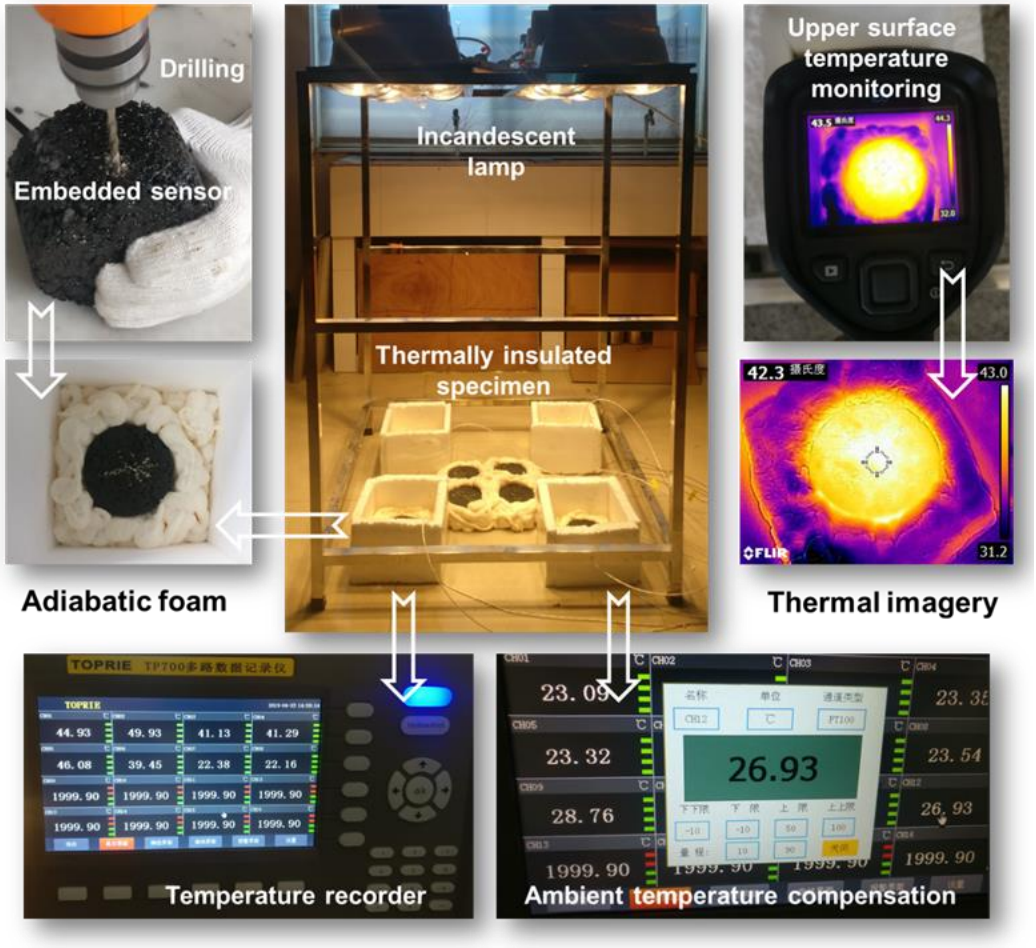

Figure 4. Irradiation test installation and temperature monitoring.

Each sample was embedded with a temperature sensor and thermally insulated by spraying foam to induce vertical heat flow. A thermal infrared imager (FLIR E6, FLIR Systems, Inc., Wilsonville, OR, USA) was used to record the temperature of the upper

surface. The temperature distributions in the mixtures were stored using a TOPRIE-TP700 recorder via an irradiation process.

3. Results and Discussion

The volumetric parameters of the asphalt mixtures with MSWIR and LF were determined using the Marshall design method (Table 4).

Table 4. Volumetric and mechanical properties.

Mixture	MS (kN)	FL (0.1 mm)	VV (%)	VMA (%)	VFA (%)	ρ (g/cm^3)
Control Mixture	12.04	30.6	4.29	17.74	74.78	2.389
Mixture #1	11.87	31.5	4.75	17.98	73.45	2.363
Mixture #2	11.81	31.3	5.31	18.41	72.44	2.331
Mixture #3	10.94	32.2	5.93	19.47	71.08	2.307
Mixture #4	10.42	32.6	6.12	20.87	70.53	2.282

The bulk density of the asphalt mixtures decreased with an increase in MSWIR content because of the lower density of the MSWIR particles compared with the LF particles. Meanwhile, the air void ratio of Mixture #4 was 1.83% higher than that of the control mixture, with higher VMA and VFA values. This phenomenon can be explained by the microstructure of the MSWIR, exhibiting spherical hollow particles, whereas the LF consisted of poriferous fragments. The differences in the volumetric parameters of the mixtures determined their thermal characteristics.

The thermal conductivity values of the specimens with different MSWIR additions were measured (Figure 1), and the testing results are listed in Table 5 to reflect the effects of the MSWIR on thermal conduction.

Table 5. Thermal conductivity of asphalt mixtures.

Mixture	λ (W/(m·K))	Testing Error (W/(m·K))
Control Mixture	1.4356	0.0206
Mixture #1	1.2964	0.0248
Mixture #2	1.2401	0.0101
Mixture #3	1.1846	0.0292
Mixture #4	1.1362	0.0052

Although the MSWIR was incorporated into the mixture by replacing an equal volume of LF, the asphalt mixtures containing MSWIR had lower thermal conductivity than the control asphalt mixture. Table 4 shows that the average thermal conductivity of Mixture #4 is 0.2994 W/(m·K) lower than that of the control mixture. These results demonstrate that the asphalt with MSWIR instead of LF had higher heat resistance.

The heat conduction characteristics of the asphalt mixture are related to its thermal conductivity and depend on its specific heat capacity. The average values of *c* are shown in Figure 5a and demonstrate that the heat storage capacity of the asphalt mixture was improved by the MSWIR. The heat storage capacity of the asphalt mixtures increased from 838.45 J/(kg·K) to 955.37 J/(kg·K) when the MSWIR completely replaced LF (Mixture #4). The increase in *c* became significant when the MSWIR was used as a substitute for at least 50% of the LF (the relative ratio of Mixture #3 is 8.1%).

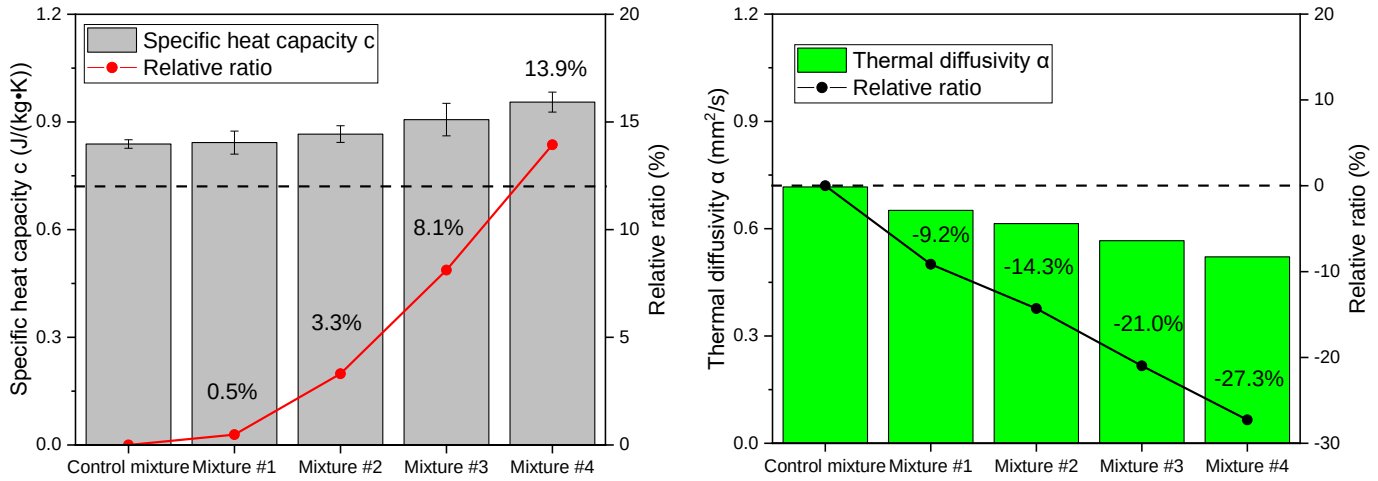

Figure 5. Thermal properties of asphalt mixtures: (**a**) specific heat capacity; (**b**) thermal diffusivity.

According to Equation (1), thermal diffusivity synthesizes the thermal properties of the material. Incorporating the MSWIR significantly improved the thermal resistance of the asphalt mixture, with a decrease in α of 0.1955 mm^2/s compared with the control mixture. An MSWIR with a hollow structure tends to prevent heat conduction, which, in this study, affected the temperature distribution of the pavement (Figure 5b). Finally, the temperatures at different depths of the asphalt mixture with MSWIR were monitored and validated using an FEM model. A set of climate data documented by a TRM-ZS1 weather station was used to validate the experimental and simulation data. The daily total solar radiation, air temperature, humidity, effective sunshine hours, air pressure, and wind speed were measured and recorded by a monitoring station using a wireless communication controller. Meteorological data measured from an asphalt road section (SMA-13) in Changsha City, China, on 27 June (Figure 6) were input into ABAQUS for full-scale thermal model validation. Furthermore, the bulk density, thermal conductivity, and specific heat capacity of the asphalt mixture were included in the model. The maximum and minimum surface temperatures were calculated using the thermal model.

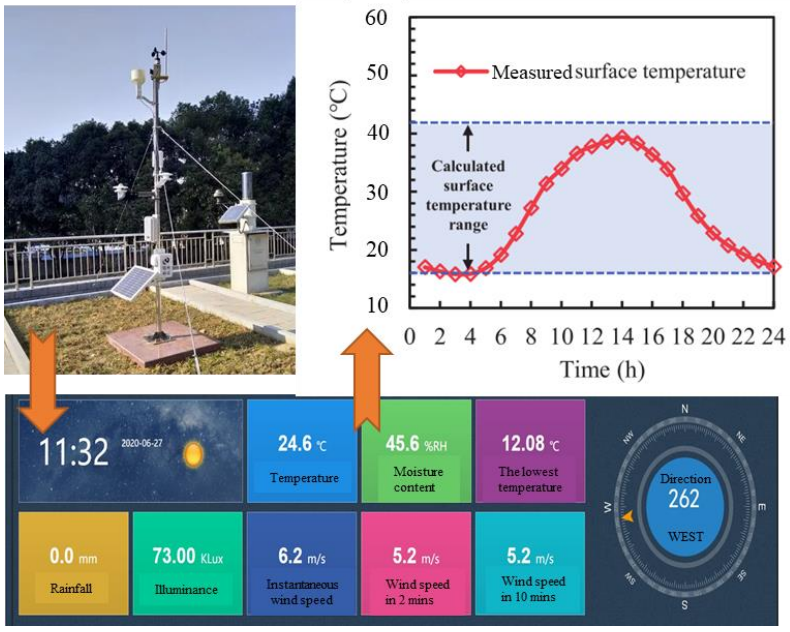

Figure 6. Meteorological data collection and temperature model validation.

Figure 6 shows how the comparison was conducted between the simulated and measured surface temperatures in order to verify the model. The surface temperature ranged from about 16 °C to 42 °C in the thermal model, and this range was comparable to the measured values. Given the solar radiation changes, the calculated maximum temperature of the surface was a little higher than the measured values, while the minimum surface temperature was approximately equal. This discrepancy is attributable to the idealization of weather parameters and material thermal properties. The close agreement between the simulated results and the field measurements indicates the reliability of the proposed thermal model in investigating the thermal behavior of asphalt mixtures. The typical weather conditions were determined to be 3.3 m/s for wind speed, 20 °C for minimum air temperature, 30 °C for maximum air temperature, 11.5 h for effective sunshine hours, and 6.747 MJ/m^2 for daily total solar radiation. The selected surface thermal conditions for the summer season and the measured thermal properties of the asphalt mixtures were adopted in the thermal field model. A hexagonal element type with linear heat transfer and tie interlayer constraints was applied during the thermal analysis. The variation and distribution of the surface and internal temperatures (Figure 7) were calculated according to the heat transfer calculation in ABAQUS for the control mixture throughout the whole day.

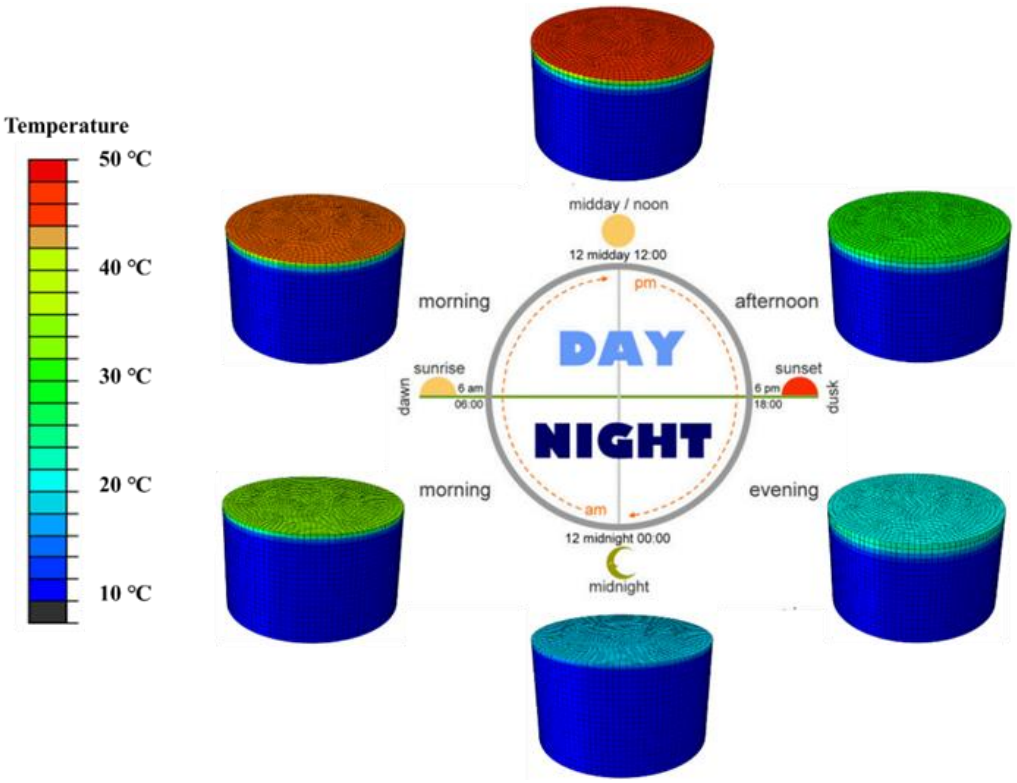

Figure 7. Surface and internal daily temperatures—control mixture.

The daily surface temperature is shown in Figure 8a,b. Given the absorbent solar radiation, the maximum surface temperature of the mixture was higher (by more than 15 °C) than the maximum daily air temperature under typical thermal conditions, which occurred at about 13:00~15:00. Conversely, the lowest surface temperature of the asphalt mixture was almost the same as the minimum daily air temperature. In addition, the mixtures including MSWIRs presented higher temperatures in the afternoon and lower temperatures at night compared with the control mixture.

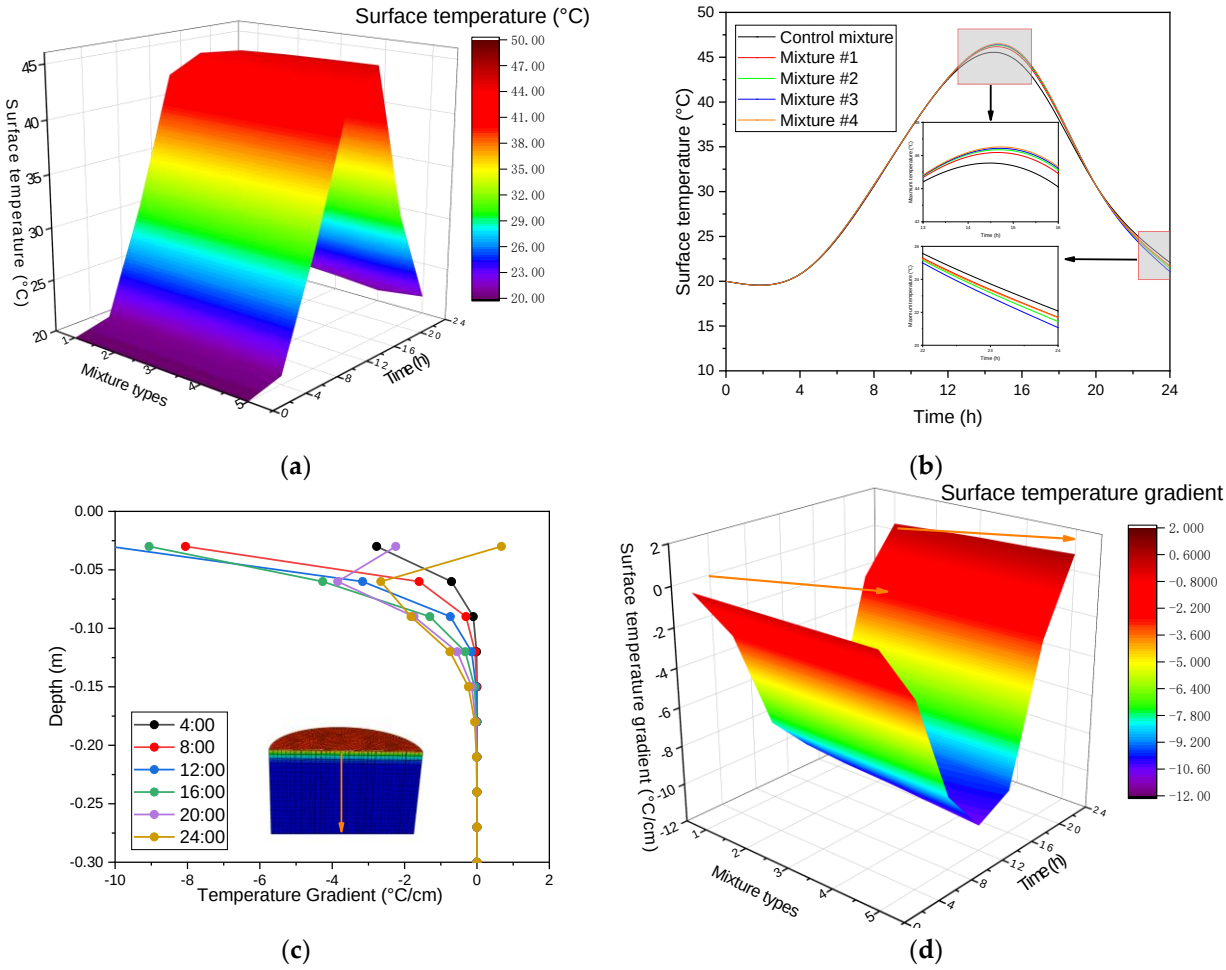

Figure 8. Finite element results: (**a**,**b**) daily maximum temperature; (**c**); daily internal temperature gradient of the control mixture; (**d**) daily surface temperature gradient of each mixture.

The variation and distribution of the internal temperature gradient at different depths of the control mixture were also recorded. Figure 8c shows that the mesh reading points were vertically distributed from the longitudinal center of the asphalt mixture. The daily variation range of the pavement temperature decreased markedly with increasing depth. The largest temperature variation was on the surface because of direct contact and heat exchange with the atmosphere [47–49].

Generally, the temperature differences between the various mixtures at the same depth resulted from the voids within the hollow microsphere structure of the MSWIR (Figure 8d). The heat conductivity of the voids was less than that of the asphalt mastics and aggregate. Therefore, the voids in the MSWIR affected the temperature distribution within the asphalt mixture, inducing a thermal resistance effect. Han et al. reported a similar finding concerning the primary heat conduction in a mixture [50]. Moreover, the temperature degradations of the asphalt mixtures represent different phenomena, which may cause micro-weather changes near pavement at night [51–53]. The main reasons for the temperature degradation difference include the thermal parameters and heat accumulation during the daytime [54,55].

Heat conduction causes heat flux gradients at different depths. These prolonged heat flux accumulations may disturb the thermal balance with the near-surface environment in urban areas. The daily heat flux evolution of the asphalt mixture based on the simulation analysis of the heat flux transfer is shown in Figure 9. The asphalt heat flux field exhibited a certain level of hysteresis in the temperature change shown in Figure 7, which contributed to the amount of flux absorbed and the conduction process.

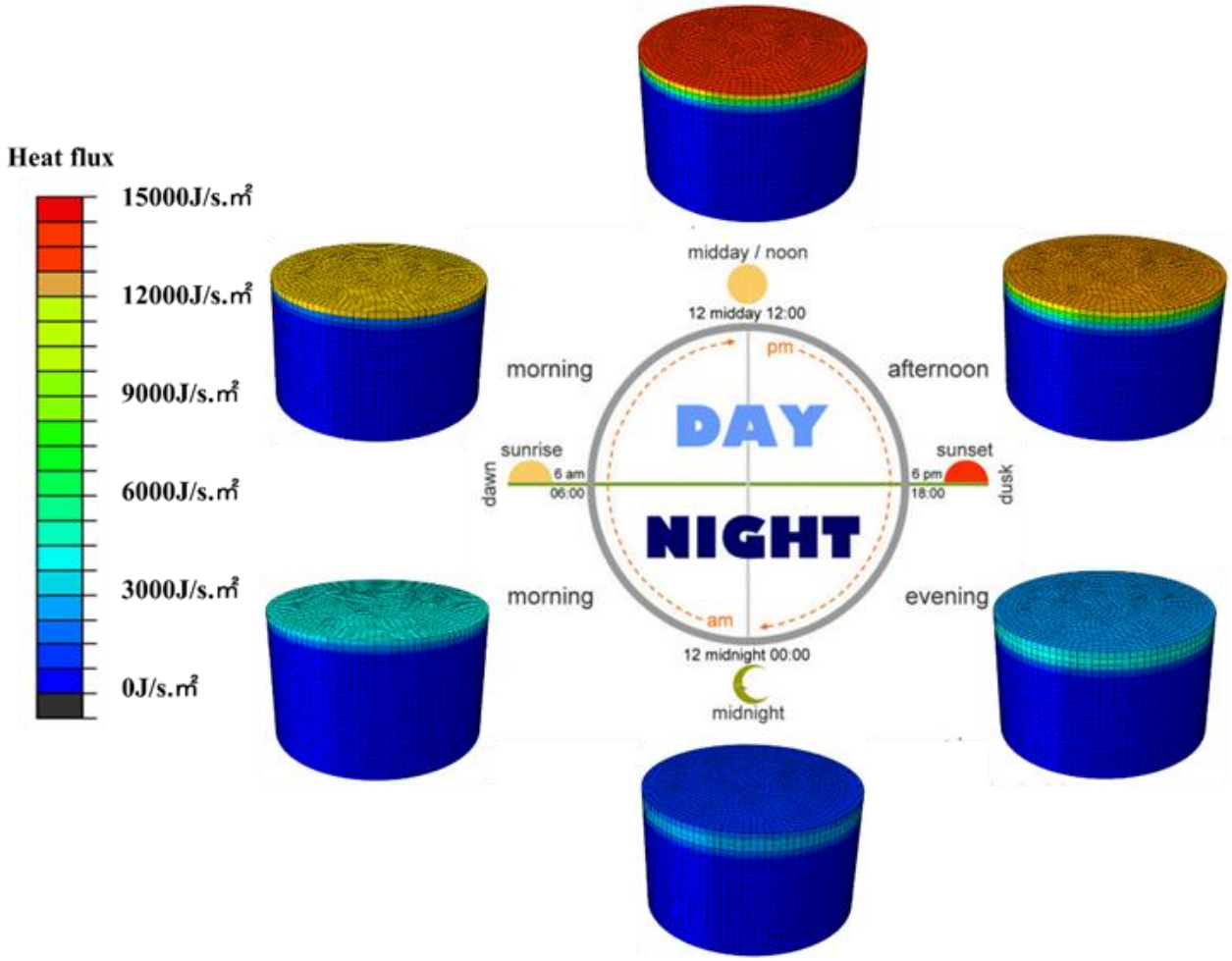

Figure 9. Surface and internal daily heat fluxes—control mixture.

Upon comparing Figure 10a,b, a time lag between the maximum temperature and the maximum heat flux can be seen in the mixture model. The heat flux gradient effect within the internal structure will change the heat transfer direction at night. This time lag phenomenon in the pavement's heat flux further affects the partial heat balance and even exacerbates heat islands [56,57].

Figure 10c,d show that the MSWIR reduced the flux gradient, indicating a higher level of thermal resistance due to lower thermal conductivity. It can be inferred that the obstruction of the transmission of heat into the in-depth layers would induce heat flux around the upper layer. Therefore, the mixture with MSWIR will exhibit a higher upper-layer temperature under the same solar radiation absorption conditions during the daytime, and less stored heat energy will be lost to the ambient environment at night. This phenomenon explains why Mixture #4 showed a larger temperature range in the daytime and a smaller temperature range at night. Therefore, it has been theoretically confirmed that the mixture with MSWIR can counter heat island effects because it releases less heat into the ambient environment at night. However, the potential heat island effect due to higher surface temperatures in the daytime cannot be overlooked.

Indoor irradiation simulated the high-temperature conditions of summer (Figure 3). This study focused on temperature evolution at different depths (i.e., 0 cm, 2 cm, 4 cm, and 6 cm below the surface). Figure 11a–c show the temperature distributions of the control mixture, Mixture #2, and Mixture #4, respectively.

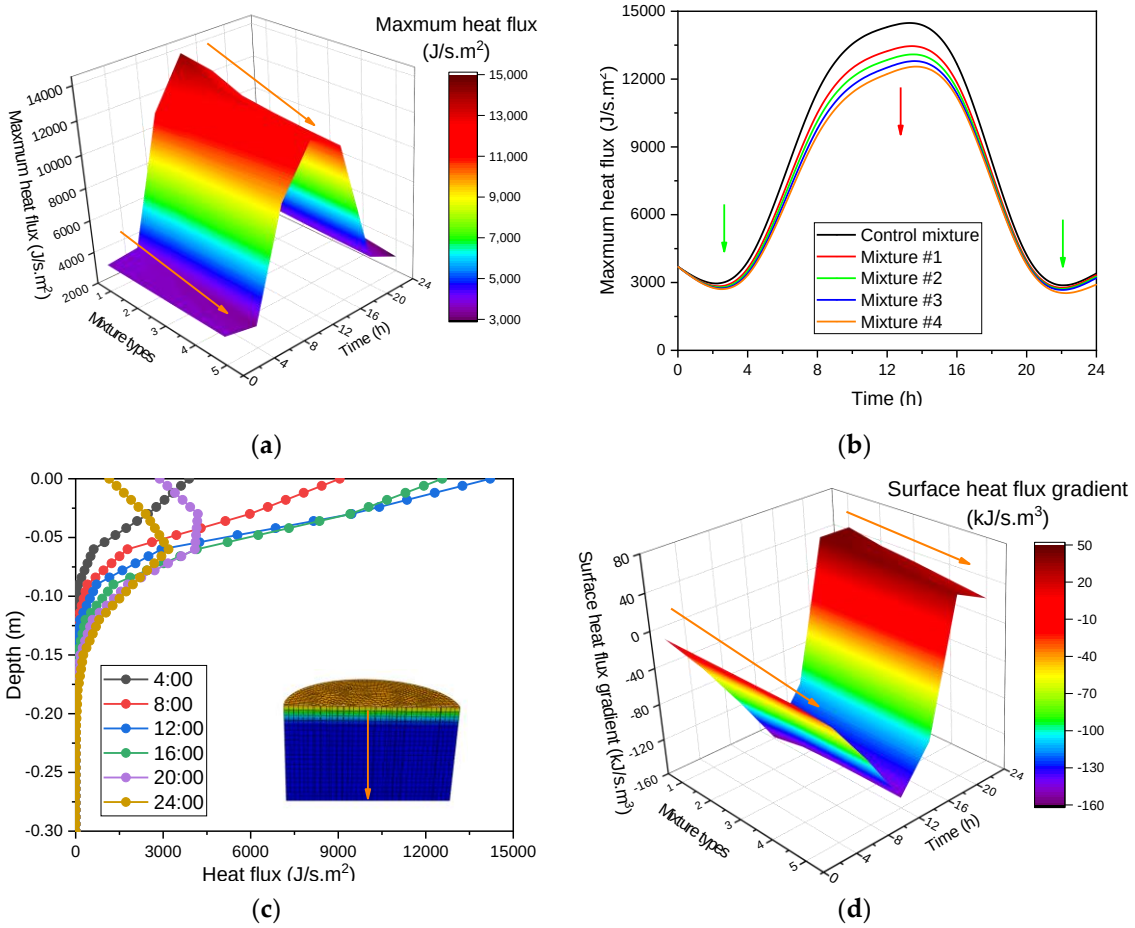

Figure 10. Finite element analysis results. (**a**,**b**) Daily maximum heat flux; (**c**) daily heat flux at different depths of the control mixture; (**d**) daily surface heat flux gradient of each mixture.

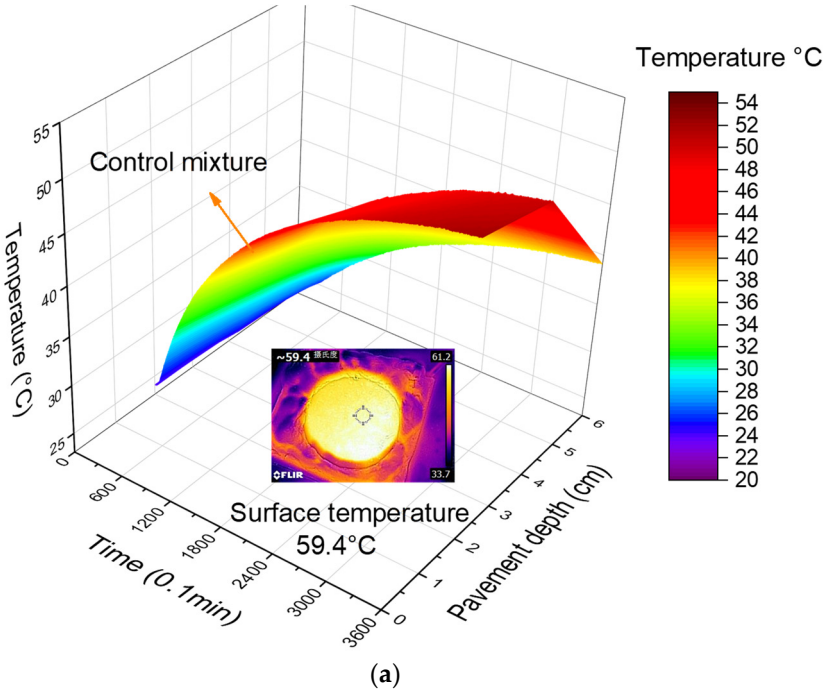

Figure 11. *Cont.*

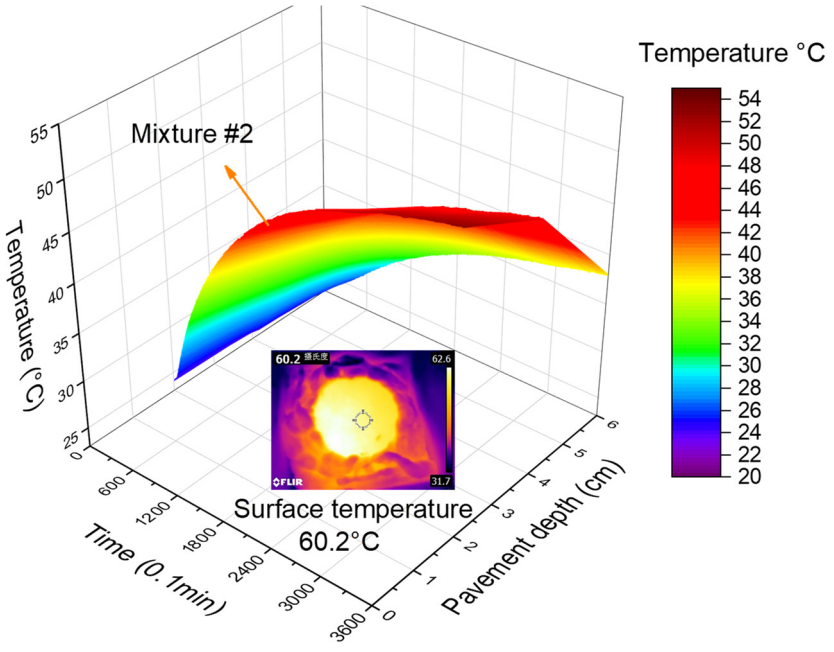

(**b**)

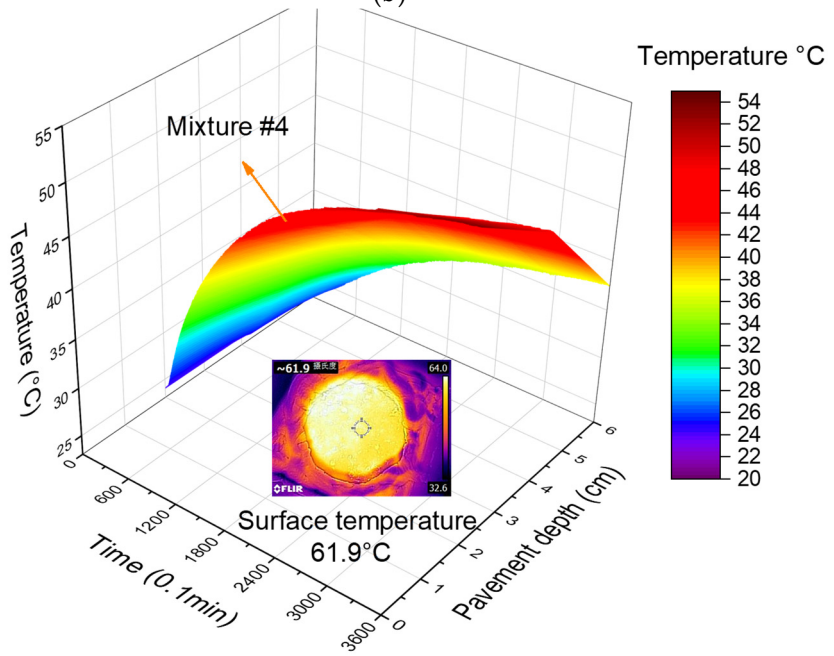

(**c**)

Figure 11. Temperature distributions: (**a**) control mixture; (**b**) Mixture #2; (**c**) Mixture #4.

Figure 11 shows that Mixture #4 had a higher average temperature than the control. The MSWIR reduced thermal diffusivity and caused more irradiation energy to accumulate. The average surface temperature increased, and the difference in surface temperature between the traditional and alternative mixtures reached up to 2.5 °C. Figure 12 shows the contrastive results of the calculated pavement temperatures.

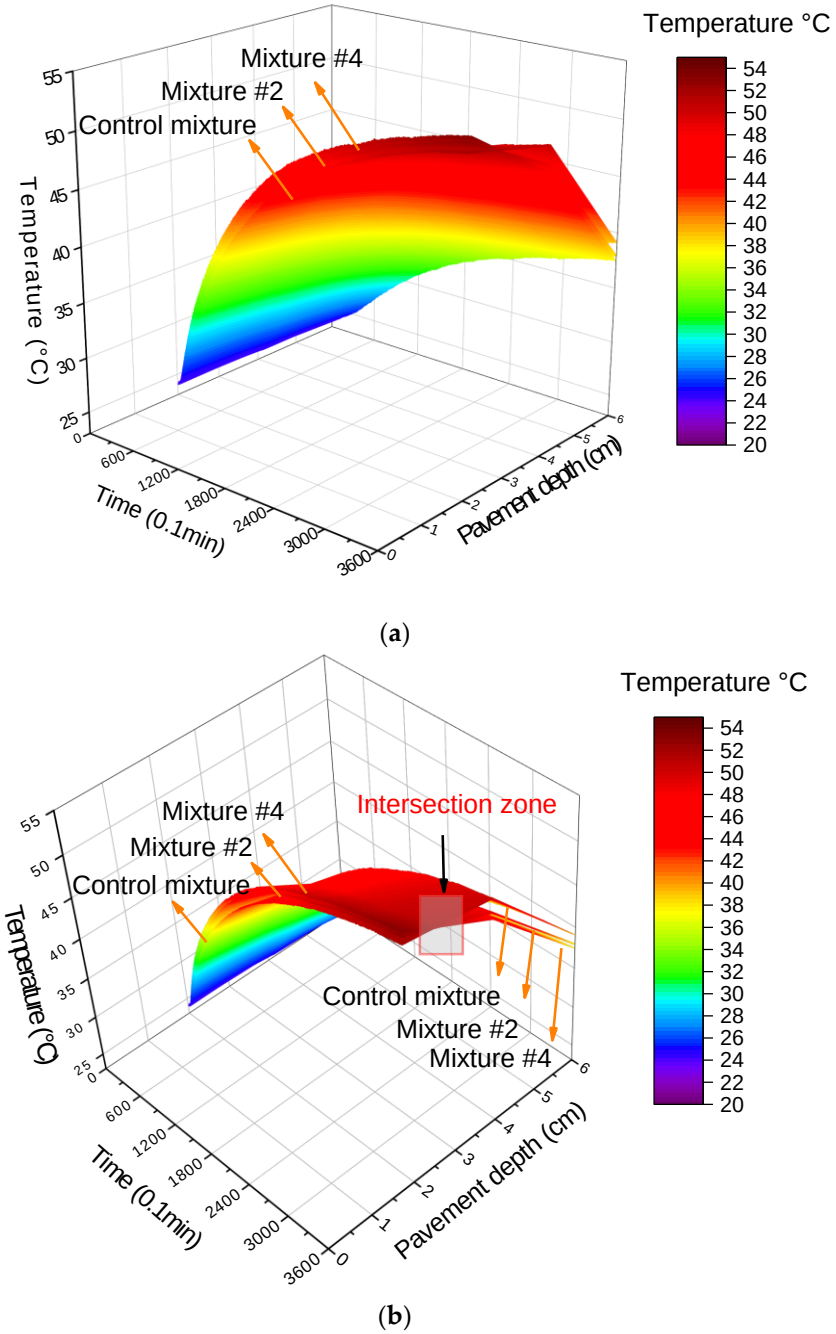

Figure 12. Comparison of temperature distributions between control mixture, Mixture #2, and Mixture #4. (**a**) Overlapped view; (**b**) Intersection zone.

Figure 12 illustrates the contrastive results for the asphalt mixtures. Incorporating MSWIR into the asphalt increased the temperature in the upper 2.5 cm thick layer. However, the temperature results at 2.5 cm to 6 cm below the surface were opposite. The temperature drop reached as low as 1.67 °C. A temperature distribution intersection zone could be observed in the three-dimensional temperature field model at a depth of 2.5 cm; this was caused by the MSWIR-to-LF ratio. This phenomenon can be explained in terms of thermal conductivity.

The temperature-monitoring results for the structural elements and the heat conduction (H_c) of the upper-layer model are shown in Figure 13. They indicate that MSWIRs in asphalt can mitigate heat accumulation inside the pavement, reducing the total heat radiation flux. An increase in the surface layer temperature might exacerbate the peak

heat island effect in urban areas. This can accelerate the convective dissipation of heat on road surfaces [58] and can be combined with urban cooling technologies [59–61] such as reflective [62,63] and evaporative pavements [64,65] and greenery [66].

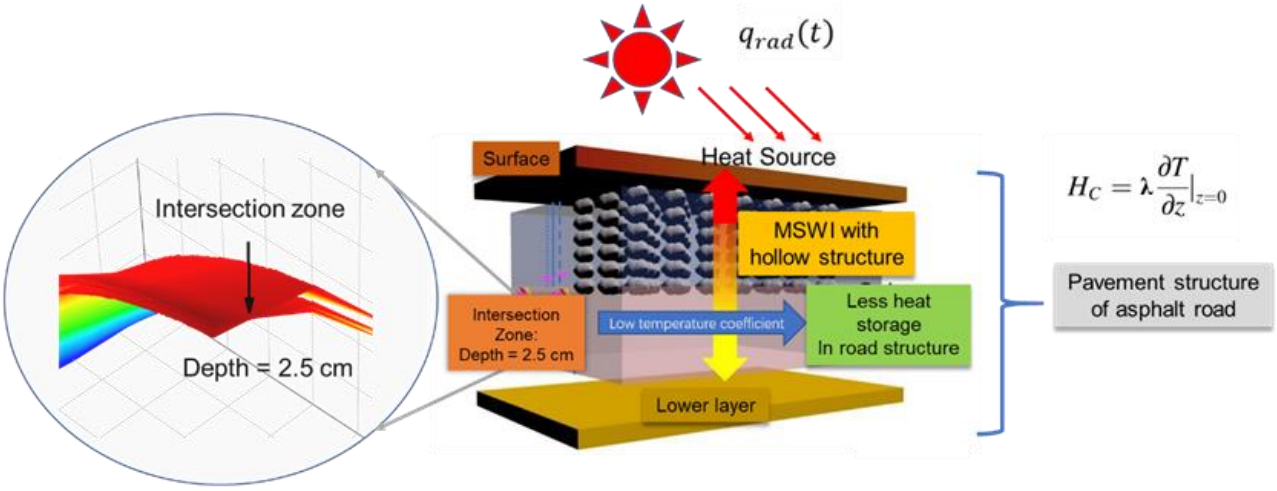

Figure 13. Structural elements and heat conduction of the upper layer.

4. Conclusions

In this study, we investigated the thermal characteristics of asphalt mixtures with MSWI residues substituting for limestone filler by varying the substitution volume between 0% and 100%. The temperature distribution within a flexible pavement was analyzed using thermal simulations and indoor irradiation tests. This research revealed the effects of an MSWIR with hollow microsphere structures on the thermal characteristics and behavior of an SMA-13 asphalt mixture. Through our numerical studies, we developed a three-dimensional finite element model describing the temperature distributions. The field investigation validated the interaction between MSWIR in flexible pavements and the urban environment.

The main conclusions are as follows:

(1) Incorporating MSWIR reduces the thermal conductivity of asphalt mixtures from 1.4356 to 1.1362 W/(m·K) compared with using LF. The specific heat capacity of the mixture increases from 0.385 to 0.9554 J/(kg·K) because of the hollow microsphere structure of the MSWI residues.

(2) Thermal diffusivity decreases by 0.1955 mm^2/s, indicating enhanced thermal resistance. Asphalt with MSWIR transfers less heat to lower layers at the same solar radiation level, which is conducive to alleviating the heat island effect.

(3) The temperature and heat flux gradients indicate a time lag for heat stored in the daytime and released at night. The heating accumulation and dissipation rate exhibit a positive correlation with the MSWIR content.

(4) Compared with the daily maximum temperature of the asphalt mixture, the daily heat flux can elucidate the thermal absorption and conductive mechanism at a more specific level, helping us to understand pavement heat transfer.

(5) The indoor irradiation test indicated the exacerbated urban heat island effect during a hot summer can cause an increase of about 2.5 °C in the surface layer temperature, which should be considered before material design and proposing MSWIR applications. Therefore, the proposed approach, combined with cool pavement technologies, can balance physical, mechanical, functional, and environmental goals.

Further studies should be conducted because this study only included SMA-13, and more asphalt mixture types should be investigated. The comprehensive performance of MSWI residues is still limited. Other testing procedures should be conducted to analyze primary properties; these procedures include fatigue and dynamic creep tests. Moreover,

we suggest deepening the investigation into the micro-mechanisms responsible for heat conduction and carrying out thermogravimetric analyses of asphalt mixtures to identify weight-loss phenomena concerning increased temperatures.

Author Contributions: Conceptualization, L.X. and M.A.; methodology, L.X. and M.A.; software, L.X. and M.A.; validation, L.M. and G.L.; formal analysis, P.P. and L.M.; investigation, L.X., L.M. and P.P.; resources, Y.D.; data curation, L.X.; writing-original draft preparation, L.X.; writing—review and editing, P.P. and L.M.; visualization, L.X.; supervision, Y.D.; project administration, Y.D.; funding acquisition, Y.D. All authors have read and agreed to the published version of the manuscript.

Funding: This research was funded by the National Natural Science Foundation of China (Grant number 51808562) and Natural Science Foundation of Hunan Province, China (Grant number 2020JJ5723).

Institutional Review Board Statement: Not applicable.

Informed Consent Statement: Not applicable.

Data Availability Statement: The data presented in this study are available on request from the corresponding author.

Conflicts of Interest: The authors declare no conflict of interest.

References

1. Elnaml, I.; Liu, J.; Mohammad, L.N.; Wasiuddin, N.; Cooper, S.B. Developing Sustainable Asphalt Mixtures Using High-Density Polyethylene Plastic Waste Material. *Sustainability* **2023**, *15*, 9897. [CrossRef]
2. Monticelli, R.; Roberto, A.; Romeo, E.; Tebaldi, G. Mixed Design Optimization of Polymer-Modified Asphalt Mixtures (PMAs) Containing Carton Plastic Packaging Wastes. *Sustainability* **2023**, *15*, 10574. [CrossRef]
3. Wong, N.H.; Jusuf, S.K.; Syafii, N.I.; Chen, Y.; Hajadi, N.; Sathyanarayanan, H.; Manickavasagam, Y.V. Evaluation of the impact of the surrounding urban morphology on building energy consumption. *Sol. Energy* **2011**, *85*, 57–71. [CrossRef]
4. Xu, L.; Magar, S.; Zhao, Z.; Xiang, Q.; Xiao, F. Rheological and anti-moisture characteristics of rubberized reclaimed asphalt pavement with interfacial bond behavior. *J. Clean. Prod.* **2023**, *391*, 136172. [CrossRef]
5. Khan, N.; Karim, F.; Latif Qureshi, Q.B.A.I.; Mufti, S.A.; Rabbani, M.B.A.; Khan, M.S.; Khan, D. Effect of Fine Aggregates and Mineral Fillers on the Permanent Deformation of Hot Mix Asphalt. *Sustainability* **2023**, *15*, 10646. [CrossRef]
6. Abbà, A.; Collivignarelli, M.C.; Sorlini, S.; Bruggi, M. On the reliability of reusing bottom ash from municipal solid waste incineration as aggregate in concrete. *Compos. Part B Eng.* **2014**, *58*, 502–509. [CrossRef]
7. Stabile, P.; Bello, M.; Petrelli, M.; Paris, E.; Carroll, M.R. Vitrification treatment of municipal solid waste bottom ash. *Waste Manag.* **2019**, *95*, 250–258. [CrossRef]
8. Cho, B.H.; Nam, B.H.; An, J.; Youn, H. Municipal Solid Waste Incineration (MSWI) Ashes as Construction Materials-A Review. *Materials* **2020**, *13*, 3143. [CrossRef]
9. Phummiphan, I.; Horpibulsuk, S.; Rachan, R.; Arulrajah, A.; Shen, S.-L.; Chindaprasirt, P. High calcium fly ash geopolymer stabilized lateritic soil and granulated blast furnace slag blends as a pavement base material. *J. Hazard. Mater.* **2018**, *341*, 257–267. [CrossRef]
10. Lynn, C.J.; Ghataora, G.S.; Obe, R.K.D. Municipal incinerated bottom ash (MIBA) characteristics and potential for use in road pavements. *Int. J. Pavement Res. Technol.* **2017**, *10*, 185–201. [CrossRef]
11. Hoy, M.; Horpibulsuk, S.; Rachan, R.; Chinkulkijniwat, A.; Arulrajah, A. Recycled asphalt pavement—Fly ash geopolymers as a sustainable pavement base material: Strength and toxic leaching investigations. *Sci. Total Environ.* **2016**, *573*, 19–26. [CrossRef]
12. Roessler, J.G.; Townsend, T.G.; Ferraro, C.C. Use of leaching tests to quantify trace element release from waste to energy bottom ash amended pavements. *J. Hazard. Mater.* **2015**, *300*, 830–837. [CrossRef] [PubMed]
13. Dou, X.; Ren, F.; Nguyen, M.Q.; Ahamed, A.; Yin, K.; Chan, W.P.; Chang, V.W.-C. Review of MSWI bottom ash utilization from perspectives of collective characterization, treatment and existing application. *Renew. Sustain. Energy Rev.* **2017**, *79*, 24–38. [CrossRef]
14. Xu, L.; Du, Y.; Loprencipe, G.; Moretti, L. Rheological and Fatigue Characteristics of Asphalt Mastics and Mixtures Containing Municipal Solid Waste Incineration (MSWI) Residues. *Sustainability* **2023**, *15*, 8356. [CrossRef]
15. del Valle-Zermeño, R.; Formosa, J.; Chimenos, J.M.; Martínez, M.; Fernández, A.I. Aggregate material formulated with MSWI bottom ash and APC fly ash for use as secondary building material. *Waste Manag.* **2013**, *33*, 621–627. [CrossRef] [PubMed]
16. Du, Y.; Ling, X.; Haibin, D.; Deyi, D.; Hao, W.; Weidong, L. Evaluation of thermal behavior and high-temperature performances of asphalt mixture containing fly ash cenosphere. *Constr. Build. Mater.* **2020**, *245*, 118429. [CrossRef]
17. Aysen Lav, M.; Hilmi Lav, A. Effects of stabilization on resilient characteristics of fly ash as pavement material. *Constr. Build. Mater.* **2014**, *54*, 10–16. [CrossRef]
18. Du, Y.; Xu, L.; Deng, H.; Deng, D.; Ma, C.; Liu, W. Characterization of thermal, high-temperature rheological and fatigue properties of asphalt mastic containing fly ash cenosphere. *Constr. Build. Mater.* **2020**, *233*, 117345. [CrossRef]

19. Del Serrone, G.; Peluso, P.; Moretti, L. Photovoltaic road pavements as a strategy for low-carbon urban infrastructures. *Heliyon* **2023**, *17*, e19977. [CrossRef]
20. Moretti, L.; Cantisani, G.; Carpiceci, M.; D'Andrea, A.; Del Serrone, G.; Di Mascio, P.; Loprencipe, G. Effect of Sampietrini Pavers on Urban Heat Islands. *Int. J. Environ. Res. Public. Health* **2021**, *18*, 13108. [CrossRef]
21. Allegrini, E.; Vadenbo, C.; Boldrin, A.; Astrup, T.F. Life cycle assessment of resource recovery from municipal solid waste incineration bottom ash. *J. Environ. Manag.* **2015**, *151*, 132–143. [CrossRef] [PubMed]
22. Kiihnl, L.; Braham, A. Exploring the influence of pavement preservation, maintenance, and rehabilitation on Arkansas' highway network: An education case study. *Int. J. Pavement Eng.* **2021**, *22*, 570–581. [CrossRef]
23. Xu, L.; Li, X.; Zong, Q.; Xiao, F. Chemical, morphological and rheological investigations of SBR/SBS modified asphalt emulsions with waterborne acrylate and polyurethane. *Constr. Build. Mater.* **2021**, *272*, 121972. [CrossRef]
24. Androutsopoulos, A.V.; Stavrakakis, G.M.; Damasiotis, M. Cool Roof Impacts on a School-building Thermal and Energy Performance in Athens, Greece. *Procedia Environ. Sci.* **2017**, *38*, 178–186. [CrossRef]
25. Xu, L.; Wang, J.; Xiao, F.; Ei-Badawy, S.; Awed, A. Potential strategies to mitigate the heat island impacts of highway pavement on megacities with considerations of energy uses. *Appl. Energy* **2021**, *281*, 116077. [CrossRef]
26. Gao, J.; Yao, Y.; Song, L.; Xu, J.; Yang, J. Determining the maximum permissible content of recycled asphalt pavement stockpile in plant hot-mix recycled asphalt mixtures considering homogeneity: A case study in China. *Case Stud. Constr. Mater.* **2022**, *16*, e00961. [CrossRef]
27. Liu, H.; Luo, R.; Xi, L.; Hu, L. Development of Two-Step Secant Method to Interpret the Flow Number Test Data of Asphalt Mixtures. *J. Mater. Civ. Eng.* **2020**, *32*, 111. [CrossRef]
28. Qin, Y.; Hiller, J.E. Understanding pavement-surface energy balance and its implications on cool pavement development. *Energy Build.* **2014**, *85*, 389–399. [CrossRef]
29. Kong, L.; Xu, L.; Du, Y.; Jin, J.; Loprencipe, G.; Moretti, L. Use of Hybrid Mineral Filler with High Emissivity in Asphalt Mixture for Cooling Road Pavements. *Materials* **2023**, *16*, 175. [CrossRef]
30. Li, Z.; Yu, X.; Liang, Y.; Wu, S. Carbon Nanomaterials for Enhancing the Thermal, Physical and Rheological Properties of Asphalt Binders. *Materials* **2021**, *14*, 2585. [CrossRef]
31. Pan, P.; Wu, S.; Xiao, Y.; Wang, P.; Liu, X. Influence of graphite on the thermal characteristics and anti-ageing properties of asphalt binder. *Constr. Build. Mater.* **2014**, *68*, 220–226. [CrossRef]
32. Liu, D.; Zhang, H.; Liu, Z.; Liu, D.; He, D.; Yu, T. The heat flux evolution of porous asphalt mixture based on *meso*-structure and its influence on heat transfer property. *Therm. Sci. Eng. Prog.* **2023**, *43*, 102020. [CrossRef]
33. Zhao, Y.; Jiang, J.; Dai, Y.; Zhou, L.; Ni, F. Thermal Property Evaluation of Porous Asphalt Concrete Based on Heterogeneous Meso-Structure Finite Element Simulation. *Appl. Sci.* **2020**, *10*, 1671. [CrossRef]
34. Hassn, A.; Aboufoul, M.; Wu, Y.; Dawson, A.; Garcia, A. Effect of air voids content on thermal properties of asphalt mixtures. *Constr. Build. Mater.* **2016**, *115*, 327–335. [CrossRef]
35. Chen, J.; Zhang, M.; Wang, H.; Li, L. Evaluation of thermal conductivity of asphalt concrete with heterogeneous microstructure. *Appl. Eng.* **2015**, *84*, 368–374. [CrossRef]
36. Mirzanamadi, R.; Johansson, P.; Grammatikos, S.A. Thermal properties of asphalt concrete: A numerical and experimental study. *Constr. Build. Mater.* **2018**, *158*, 774–785. [CrossRef]
37. Mu, K.; Chen, J.; Mu, Q.; Garg, A.; Gao, Z.; Li, Y. Development of a microstructure-based numerical approach for analyzing heat transfer within the asphalt mixture. *Constr. Build. Mater.* **2020**, *260*, 119890. [CrossRef]
38. Jiang, L.; Wang, S.; Gu, X.; Dorjee, N.; Bo, W. Inducing directional heat transfer by enhancing directional thermal conductivity of asphalt mixtures for improving asphalt solar collectors. *Constr. Build. Mater.* **2021**, *267*, 121731. [CrossRef]
39. Li, Z.; Wang, S. Transferring heat accumulated by asphalt pavement from inside to outside through carbon fibers. *Constr. Build. Mater.* **2023**, *383*, 131314. [CrossRef]
40. Shamsaei, M.; Carter, A.; Vaillancourt, M. A Review on the Heat Transfer in Asphalt Pavements and Urban Heat Island Mitigation Methods. *Constr. Build. Mater.* **2022**, *359*, 129350. [CrossRef]
41. Górszczyk, J.; Malicki, K. Comparison of temperature distributions in road pavement obtained in field tests and using transient thermal analysis. *MATEC Web Conf.* **2019**, *262*, 05007. [CrossRef]
42. Balreddy, M.S.; Nethra, P.; Naganna, S.R. Performance Evaluation of Open-Graded Bituminous Concrete Modified with Natural Fibers. *Sustainability* **2023**, *15*, 11952. [CrossRef]
43. Khorshidi, M.; Goli, A.; Orešković, M.; Khayambashi, K.; Ameri, M. Performance Evaluation of Asphalt Mixtures Containing Different Proportions of Alternative Materials. *Sustainability* **2023**, *15*, 13314. [CrossRef]
44. *JTG E20-2011*; Standard Test Methods of Bitumen and Bituminous Mixtures for Highway Engineering. Chinese Standard: Beijing, China, 2011.
45. *JTG E42-2005*; Test Methods of Aggregate for Highway Engineering. Chinese Standard: Beijing, China, 2004.
46. *JTG F40-2004*; Technical Specifications for Construction of Highway Asphalt Pavements. Chinese Standard: Beijing, China, 2004.
47. Hatvani-Kovacs, G.; Belusko, M.; Skinner, N.; Pockett, J.; Boland, J. Heat stress risk and resilience in the urban environment. *Sustain. Cities Soc.* **2016**, *26*, 278–288. [CrossRef]
48. He, Q.; Tapia, F.; Reith, A. Quantifying the influence of nature-based solutions on building cooling and heating energy demand: A climate specific review. *Renew. Sustain. Energy Rev.* **2023**, *186*, 113660. [CrossRef]

49. Rossi, F.; Pisello, A.L.; Nicolini, A.; Filipponi, M.; Palombo, M. Analysis of retro-reflective surfaces for urban heat island mitigation: A new analytical model. *Appl. Energy* **2014**, *114*, 621–631. [CrossRef]
50. Han, D.; Liu, G.; Zhao, Y.; Pan, Y.; Yang, T. Research on thermal properties and heat transfer of asphalt mixture based on 3D random reconstruction technique. *Constr. Build. Mater.* **2021**, *270*, 121393. [CrossRef]
51. Buchin, O.; Hoelscher, M.-T.; Meier, F.; Nehls, T.; Ziegler, F. Evaluation of the health-risk reduction potential of countermeasures to urban heat islands. *Energy Build.* **2016**, *114*, 27–37. [CrossRef]
52. Sheng, L.; Tang, X.; You, H.; Gu, Q.; Hu, H. Comparison of the urban heat island intensity quantified by using air temperature and Landsat land surface temperature in Hangzhou, China. *Ecol. Indic.* **2017**, *72*, 738–746. [CrossRef]
53. Santamouris, M.; Cartalis, C.; Synnefa, A.; Kolokotsa, D. On the impact of urban heat island and global warming on the power demand and electricity consumption of buildings—A review. *Energy Build.* **2015**, *98*, 119–124. [CrossRef]
54. Fernández, F.J.; Alvarez-Vázquez, L.J.; García-Chan, N.; Martínez, A.; Vázquez-Méndez, M.E. Optimal location of green zones in metropolitan areas to control the urban heat island. *J. Comput. Appl. Math.* **2015**, *289*, 412–425. [CrossRef]
55. Wang, Y.; Berardi, U.; Akbari, H. Comparing the effects of urban heat island mitigation strategies for Toronto, Canada. *Energy Build.* **2016**, *114*, 2–19. [CrossRef]
56. Akbari, H.; Matthews, H.D. Global cooling updates: Reflective roofs and pavements. *Energy Build.* **2012**, *55*, 2–6. [CrossRef]
57. Santamouris, M.; Ban-Weiss, G.; Osmond, P.; Paolini, R.; Synnefa, A.; Cartalis, C.; Muscio, A.; Zinzi, M.; Morakinyo, T.E.; Ng, E.; et al. Progress in urban greenery mitigation science—Assessment methodologies advanced technologies and impact on cities. *J. Civ. Eng. Manag.* **2018**, *24*, 638–671. [CrossRef]
58. Hendel, M.; Parison, S.; Grados, A.; Royon, L. Which pavement structures are best suited to limiting the UHI effect? A laboratory-scale study of Parisian pavement structures. *Build. Environ.* **2018**, *144*, 216–229. [CrossRef]
59. Besir, A.B.; Cuce, E. Green roofs and facades: A comprehensive review. *Renew. Sustain. Energy Rev.* **2018**, *82*, 915–939. [CrossRef]
60. Akbari, H.; Kolokotsa, D. Three decades of urban heat islands and mitigation technologies research. *Energy Build.* **2016**, *133*, 834–842. [CrossRef]
61. Qin, Y. A review on the development of cool pavements to mitigate urban heat island effect. *Renew. Sustain. Energy Rev.* **2015**, *52*, 445–459. [CrossRef]
62. Cheela, V.R.S.; John, M.; Biswas, W.; Sarker, P. Combating Urban Heat Island Effect—A Review of Reflective Pavements and Tree Shading Strategies. *Buildings* **2021**, *11*, 93. [CrossRef]
63. Kyriakodis, G.-E.; Santamouris, M. Using reflective pavements to mitigate urban heat island in warm climates—Results from a large scale urban mitigation project. *Urban. Clim.* **2018**, *24*, 326–339. [CrossRef]
64. Manteghi, G.; Mostofa, T. Evaporative Pavements as an Urban Heat Island (UHI) Mitigation Strategy: A Review. *Int. Trans. J. Eng. Manag. Appl. Sci. Technol.* **2019**, *11*, 1–15. [CrossRef]
65. Wang, J.; Meng, Q.; Tan, K.; Santamouris, M. Evaporative cooling performance estimation of pervious pavement based on evaporation resistance. *Build. Environ.* **2022**, *217*, 109083. [CrossRef]
66. Peluso, P.; Persichetti, G.; Moretti, L. Effectiveness of Road Cool Pavements, Greenery, and Canopies to Reduce the Urban Heat Island Effects. *Sustainability* **2022**, *14*, 16027. [CrossRef]